

5-17

2620 Lett

UNCLASSIFIED

NRL Report 8284

Electromagnetic Scattering Patterns from Sinusoidal Surfaces

A.K. JORDAN AND R.H. LANG

*Aerospace Systems Branch
Space Systems Division*

April 10, 1979



**NAVAL RESEARCH LABORATORY
Washington, D.C.**

Approved for public release; distribution unlimited.

20. ABSTRACT (Continued)

plotted for a variety of surface parameters. The present method for scattering-pattern calculations can be considered to be complementary to methods using physical-optics and point-matching techniques. In addition to presenting the scattering-pattern calculations, the report includes the computation of the exact Bragg backscattering amplitudes and compares them to their Rayleigh approximations.

CONTENTS

INTRODUCTION	1
REPRESENTATION OF THE ELECTROMAGNETIC FIELD	2
CALCULATION OF THE SCATTERING PATTERNS	6
DISCUSSION	14
ACKNOWLEDGMENTS	15
REFERENCES	15

ELECTROMAGNETIC SCATTERING PATTERNS FROM SINUSOIDAL SURFACES

INTRODUCTION

Electromagnetic waves that are scattered from rough surfaces have a characteristic dependence on the observation angle. In addition to scattering at the specular angle, which is characteristic of reflection from a smooth plane, these waves also scatter at many different angles, due to the rough nonplanar nature of the surface. In this paper we present an analysis and calculation of scattering patterns from a sinusoidal surface, which is the prototype of a periodic rough surface. An exact representation of the electromagnetic field is used to calculate scattering patterns from a finite illuminated area of the surface. A motivation for this study has been the investigation of the effects of sea clutter on radar target identification procedures.

Scattering from rough surfaces has been calculated with the space-harmonic representation which expresses the scattered field as a discrete sum of space harmonics (plane waves). The scattering coefficient associated with each space harmonic is calculated after the application of an exact boundary condition on the surface. The formulation which we use was provided by DeSanto [1] and is similar to the analysis by Uretsky [2]. Direct numerical solution of the integral equation for the surface current has been made by Zaki and Neureuther [3] and by Tong and Senior [4]. Whitman and Schwering [5] have independently obtained a formulation similar to that of DeSanto [1] and furthermore have compared their calculations with the direct numerical solutions cited above. Waterman [6] has calculated the scattering coefficients by solving the matrix equations for the surface fields.

In principle, the space-harmonic representation is exact; however, simple approximate representations for the scattering coefficients can be obtained if the perturbation (Rayleigh-Rice) approximation [7] is used. This procedure has been used by Valenzuela [8], Wright [9], Barrick [10], and Rosich and Wait [11] to explain the phenomenon of Bragg scattering of microwaves from slightly rough surfaces such as the ocean.

The physical-optics (Kirchhoff) approximation is an alternate method, which assumes that the surface field is equivalent to the field which would be induced on a local tangent plane. The scattered field is found by integration over the illuminated area. Scattered fields have been calculated with this method by Beckmann and Spizzichino [12] and Senior [13]. Lentz [14] in particular has compared scattering patterns calculated with the physical-optics method, direct numerical evaluation of the integrals, and perturbation methods. Backscattering from composite rough surfaces has been analyzed by Fung and Chan [15]. Reviews of the methods which

have been applied to calculate scattering from random rough surfaces have been published by Valenzuela [16], Shmelev [17], and Beckmann and Spizzichino [12].

REPRESENTATION OF THE ELECTROMAGNETIC FIELD

The electromagnetic field scattered from a sinusoidal surface is represented by a superposition of plane waves which consists of a discrete spectrum of space harmonics. The analysis is briefly summarized here in order to define our notation and to display the working formulas.

The electromagnetic field is assumed to be horizontally polarized so that the plane of incidence is the $x-z$ plane and the E-field is parallel to the y -axis: $\mathbf{E} = \hat{\mathbf{y}} \psi(x, z)$ with $\hat{\mathbf{y}}$ being a unit vector in the y direction. The analysis for vertically polarized fields proceeds similarly [1]. The total field amplitude $\psi(x, z)$ above the $z = 0$ plane is composed of the incident and scattered field amplitudes

$$\psi(x, z) = \psi_o(x, z) + \psi_{sc}(x, z), \quad z \geq 0. \quad (1)$$

The spatial dependence of the incident plane wave is

$$\psi_o(x, z) = e^{ik(\alpha_o x - \beta_o z)}, \quad z \geq 0, \quad (2)$$

where $k = 2\pi/\lambda$ is the wavenumber and $\alpha_o = \sin \theta_o$, $\beta_o = \cos \theta_o$. The space-harmonic representation of the scattered field is

$$\psi_{sc}(x, z) = \sum_{n=-\infty}^{\infty} A_n e^{ik(\alpha_n x - \beta_n z)}, \quad z \geq 0 \quad (3)$$

where A_n is the scattering coefficient of the n th space harmonic, $\alpha_n = \sin \theta_n$, $\beta_n = \cos \theta_n$, and θ_n is the scattering angle of the n th space harmonic.

The profile $s(x)$ of the surface shown in Fig. 1 is a sinusoid with period l and roughness amplitude d :

$$s(x) = -\frac{d}{2} \left[1 + \cos \frac{2\pi}{l} x \right]. \quad (4)$$

Due to the periodicity of the boundary-value problem,

$$\alpha_n = \alpha_o + n\Lambda, \quad n = \pm 1, \pm 2, \dots, \quad (5)$$

where $\Lambda = \lambda/l$, so that

$$\beta_n = \sqrt{1 - \alpha_n^2}, \quad \text{Im}(\beta_n) \geq 0, \quad (6)$$

is complex in general. The scattering coefficient A_n can be calculated by applying Green's theorem with the Dirichlet boundary condition on $s(x)$,

$$\psi[x, s(x)] = 0, \quad (7)$$

to obtain the integral equation

$$-\int_C G^\pm \frac{\partial \psi}{\partial n} d\mu = 0, \quad (8)$$

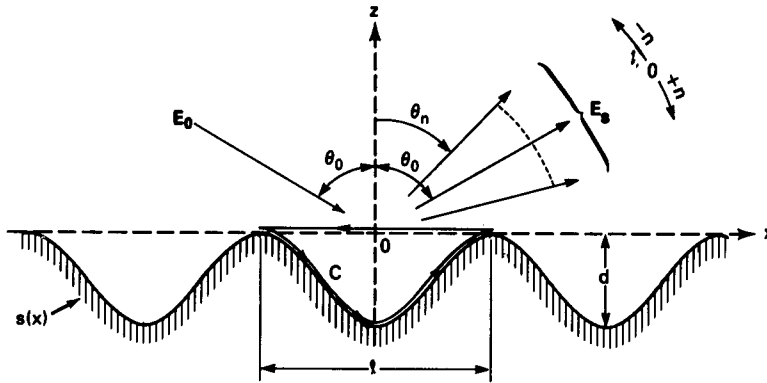


Fig. 1— Plane-wave scattering by a sinusoidal surface $s(x)$

where

$$G^\pm = e^{ik(\pm\beta_n z - \alpha_n x)}, \tag{9}$$

μ is the arc length along the contour C of Fig. 1, and n is the inward-drawn normal. The integral is evaluated along the contour C by using only the assumption that $\partial\psi/\partial n$ is periodic, so that the Rayleigh hypothesis [18] is not used. The results are [1]

$$A_m = -\frac{\beta_0}{\beta_m} i^m e^{i\tau_m^+} \left[J_m(\tau_m^+) + \sum_{n \neq 0} a_n J_{m-n}(\tau_m^+) \right], \quad m = 0, 1, \pm 2, \dots, \tag{10}$$

where the a_n are the solutions of the set of equations

$$J_m(\tau_m^-) + \sum_{n \neq 0} a_n J_{m-n}(\tau_m^-) = 0, \quad m = \pm 1, \pm 2, \dots, \tag{11}$$

$J_m(\tau_m^\pm)$ is the m th-order Bessel function, $\tau_m^\pm = \Delta(\beta_0 \pm \beta_m)$, and $\Delta = \pi d/\lambda$. The a_n are the coefficients of the Fourier expansion of the surface currents and thus may be called surface current amplitudes. The usual Rayleigh amplitude approximation is found by setting $a_n = 0$ for all $n \neq 0$ in Eq. (10).

The infinite set of linear equations (11) can be solved numerically for the a_n , $n = \pm 1, \pm 2, \dots$, by symmetrically truncating the system at an order M and solving the resulting $2M$ -order matrix equation; this technique is known as the method of reduction. However, as has been pointed out by Holford [19], the usual techniques for showing that the method of reduction converges cannot be employed unless the system of equations (11) can be represented in matrix form as $(\mathbf{I} + \mathbf{J}) \cdot \mathbf{a} = \mathbf{O}$, where \mathbf{I} is the identity matrix, \mathbf{O} is the zero vector, \mathbf{a} is the vector of the unknown surface current amplitudes $\{a_n\}$, and \mathbf{J} is a matrix having a bounded norm. It can be shown for our case that the norm of \mathbf{J} is not bounded and thus we cannot employ standard theory to guarantee convergence.

Confidence in our numerical method for solving the set of equations (11) for the surface current amplitudes was established by employing two criteria:

(i) Conservation of energy. The normalized energy density in the n th space harmonic at the plane $z = z_0 > 0$ is

$$|R_n|^2 = |A_n|^2 \frac{\beta_n}{\beta_0}. \quad (12)$$

Since the total incident energy density was normalized, conservation of energy in the plane $z = z_0$ requires that

$$\int_{-1/2}^{1/2} |\psi_{sc}(x)|^2 dx = 1. \quad (13)$$

The energy conservation criterion which we compute is

$$\lim_{M \rightarrow \infty} \left| 1 - \sum_{n \in P} |R_n(M)|^2 \right| = \lim_{M \rightarrow \infty} \epsilon_M = 0, \quad (14)$$

where $R_n(M)$ means the approximation to R_n obtained when the $\{a_n\}$ are computed after truncating the set of equations (11) at order M . The sum is only over the set of propagating modes $P = \{n: \text{Im}(\beta_n) = 0\}$, since the set of evanescent modes $E = \{n: \text{Im}(\beta_n) > 0\}$ does not contribute to the radiated energy. However, the calculation of the set of surface current amplitudes $\{a_n\}$ from the linear equations (11) requires both sets P and E , since the near-field distribution of the total energy among the various space harmonics is influenced by the evanescent modes. These modes include such effects as shadowing, diffraction, and multiple scattering, and will influence the values of the scattering coefficients so that including more space harmonics as $M \rightarrow \infty$ will increase the accuracy of the $\{a_n\}$ and also the $\{A_n\}$. The energy-conservation errors ϵ_M for several illustrative examples are given in Table 1 together with the corresponding matrix orders $2M$ for both the Rayleigh approximation and the exact representation.

Table 1 — Parameters for Scattering-Pattern Calculations

Example	Λ	Δ	σ_m	θ_0 (deg)	Perturbation Condition (Eq. (18))	Physical- Optics Condition (Eq. (19))	No. of Propagat- ing Modes	Matrix Order $2M$	Energy conservation error ϵ_M	
									Rayleigh approx.	Exact represent.
1	0.40	2.356	0.942	45	0.555	1.234	5	28	0.631	8.58×10^{-8}
2	0.10	3.00	0.30	45	0.555	992.96	20	36	0.125	8.88×10^{-16}
3	$\sqrt{2}$	1.50	2.121	45	0.555	1.914	2	22	0.656	1.10×10^{-6}
4	$\sqrt{27/2}$	1.11	0.785	45	0.555	0.432	3	18	0.476	2.71×10^{-8}
5	0.40	2.356	0.942	11.536	0.400	23.98	6	30	2.95×10^{-7}	1.66×10^{-9}

(ii) Stability of matrix solutions. The complex values of a symmetric subset of the surface current amplitudes $\{a_n\}$ should stabilize with increasing matrix size $2M$ for a given set of parameters $\Lambda, \Delta, \theta_0$. In all cases which we examined, the energy-conservation and current-stabilization criteria were compatible.

The numerical examples summarized in Table 1 were chosen to demonstrate several interesting scattering phenomena and to compare our results with previously published results. The table also serves to relate the scattering patterns of the next section with the analysis of the scattering coefficients in the present section. We have chosen three of the examples to demonstrate two phenomena whose space-harmonic representations have been extensively studied, but which have not been related to the corresponding scattering patterns. The first of these phenomena is n th-order resonant Bragg backscattering. The Bragg angles θ_{Bn} are found from Eq. (5) with $\alpha_n = -\alpha_0$,

$$\theta_{Bn} = \sin^{-1} \left(\frac{n\Lambda}{2} \right), \quad n = -1, -2, \dots \quad (15)$$

The second phenomenon is anomalous behavior in the scattering coefficients which occurs at the Rayleigh-Wood angles, $\theta_{Wn} = -\arcsin(n\Lambda \pm 1)$ [20].

The examples were also chosen to demonstrate the accuracy of our calculations for profiles whose parameters exceed the conditions for two previously-used approximations, which are

(i) Perturbation (Rayleigh-Rice) approximation. A surface is "slightly rough" if both its maximum slope and its roughness amplitude are small enough. The condition on the slope has been obtained by Millar [18], who showed that the Rayleigh hypothesis is satisfied if the maximum slope of a sinusoidal surface

$$\sigma_m = \left. \frac{d}{dx} s(x) \right|_{\max} = \frac{\pi d}{l} = \Delta \Lambda, \quad (16)$$

satisfies the condition

$$0.448 > \sigma_m. \quad (17)$$

In addition, if the roughness amplitude is small enough, e.g.

$$\Delta < \frac{\pi}{8 \cos \theta_0}, \quad (18)$$

then perturbation methods can be used to calculate the reflection coefficients R_n [7].

(ii) Physical-optics (Kirchhoff) approximation. Beckmann and Spizzichino ([12], Eq. (4.3.11)) have shown that the physical-optics approximation can be applied to a sinusoidal surface if no shadowing occurs and if the minimum radius of curvature is large enough; in our notation,

$$1 \ll \frac{2\pi}{\Lambda^3 \Delta} \cos(\theta_0 + \arctan \Delta \Lambda). \quad (19)$$

Neither approximation was used in the derivation of the scattering coefficients (Eq. (10)) and, as shown in Table 1, which lists the values of the right-hand sides of Eqs. (17), (18), and (19), the energy-conservation criterion is satisfied by surfaces that exceed these conditions, if the exact representation is used.

Example 1 is similar to an example of Whitman and Schwering ([5], Fig. 3) and we have verified their calculations. Both the perturbation and physical-optics conditions are exceeded.

Example 2 is similar to an example of Beckmann and Spizzichino ([12], Fig. 4.7) and compares the space-harmonic with the physical-optics calculations. Since Λ is small there are many propagating modes (20 in this case); although the energy-conservation criterion is satisfied here, the space-harmonic representation will become unwieldy for $\Lambda \ll 1$ and the physical-optics method will be more appropriate for those cases where the radius of curvature is large.

Example 3 demonstrates first-order Bragg backscattering and Example 4 demonstrates second-order Bragg backscattering for surfaces that exceed the "slightly-rough" conditions of Eqs. (17) and (18).

Example 5 demonstrates the Rayleigh-Wood anomalies. The incidence angle of Example 1 has been adjusted so that $\theta_2 = +90^\circ$ and $\theta_{-3} = -90^\circ$; θ_{-1} is a first-order Bragg backscattering angle. Although the energy-conservation error suggests that the Rayleigh approximation is somewhat apocryphal, the exact representation seems valid.

Because of the interest in radar backscatter, we have used our technique to investigate the behavior of the Bragg backscattering amplitude $\sqrt{R_{-1}(\theta_0)}$. Plots of $\sqrt{R_{-1}(\theta_0)}$ as a function of the normalized roughness amplitude Δ are shown in Fig. 2 for several values of θ_0 . It is seen that for small values of Δ the Bragg backscattering amplitude depends linearly on Δ , which agrees with the predictions of first-order perturbation theory [8]. For larger values of Δ and angles that are not too close to grazing, the curves tend to follow an oscillatory pattern. As the angle of incidence is increased toward grazing, the amplitude of the oscillation tends to zero and the curves appear to saturate. In addition, the Rayleigh approximations to the Bragg backscattering amplitudes have been plotted. They depart significantly from the exact representation for surface slopes greater than one. The Rayleigh approximations also exhibit the "Brewster-angle effect" when the backscattered amplitudes vanish at the zeros of the corresponding Bessel functions.

CALCULATION OF THE SCATTERING PATTERNS

Scattering patterns from sinusoidal surfaces can be calculated if the scattered fields are known on a finite illuminated area of the surface. Here a scattering pattern is defined as the graph of the scattered electromagnetic energy density as a function of the observation angle. In general, the incident electromagnetic field has a spherical wavefront due to a point source at a finite distance. For numerical simplicity, we will use an approximate calculation of scattering patterns with an incident beam of plane waves; the implications of this approximation will be discussed in the next section.

The incident field has a finite beamwidth, as shown in Fig. 3, and can be represented in the $z = 0$ plane by a continuum of plane waves

$$\psi_i(x, 0) = \int_{-\infty}^{\infty} B(\alpha_0) e^{ik\alpha_0 x} d\alpha_0, \quad (20)$$

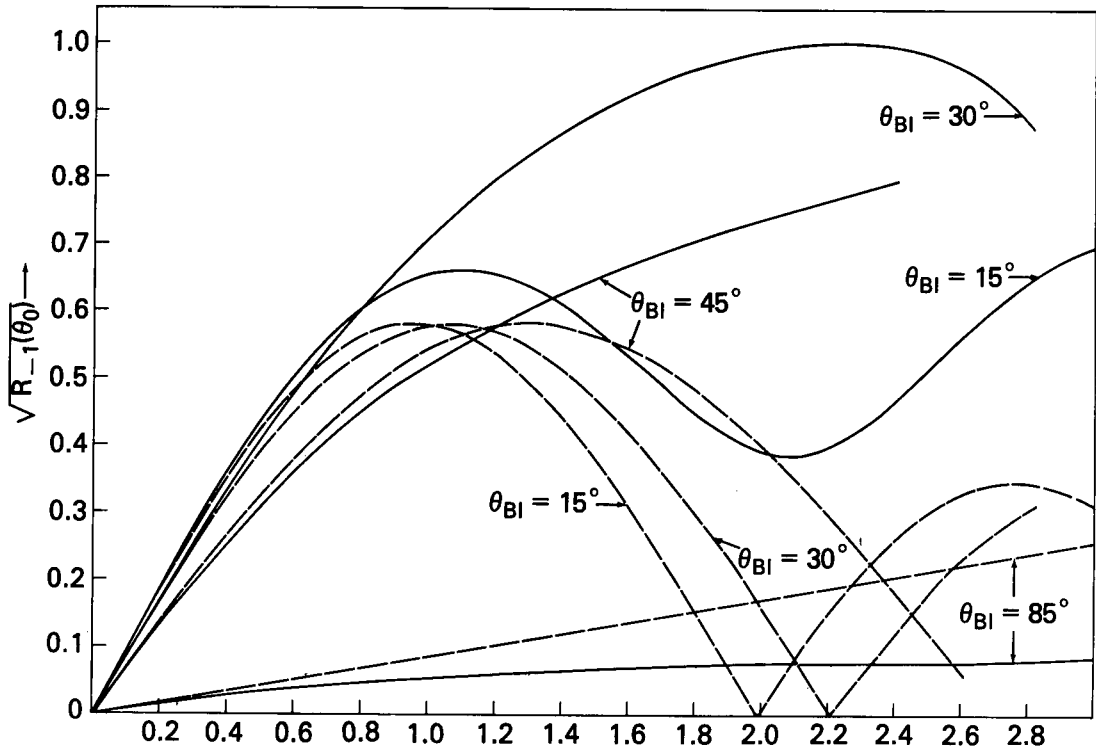


Fig. 2—Bragg backscattering amplitude $\sqrt{R_{-1}(\theta_0)}$ as a function of roughness parameter Δ . Solid curves correspond to the exact representation, dashed curves correspond to the Rayleigh approximation. The Bragg backscattering angles θ_{BI} are defined by Eq. (15).

where the Fourier components of $\psi_i(x, 0)$ are

$$B(\alpha_o) = \frac{1}{2\pi} \int_{-\infty}^{\infty} \psi_i(x, 0) e^{-ik\alpha_o x} dx. \quad (21)$$

The resultant scattered field can be represented as a superposition of scattered space harmonics,

$$\psi_{sc}(x, z) = \int_{-\infty}^{\infty} B(\alpha_o) \psi_{sc}(x, z; \alpha_o) d\alpha_o, \quad (22)$$

where $\psi_{sc}(x, z; \alpha_o)$ is the scattered-field amplitude due to a unit amplitude plane wave incident upon the surface with a direction cosine α_o . If the expression for ψ_{sc} given by Eq. (3) is used in Eq. (22), the scattered field is found to be

$$\psi_{sc}(x, z) = \sum_{n=-\infty}^{\infty} \psi_{sc}^{(n)}(x, z), \quad (23)$$

where

$$\psi_{sc}^{(n)}(x, z) = \int_{-\infty}^{\infty} B(\alpha_o) R_n(\alpha_o) e^{ik(\alpha_n x + \beta_n z)} d\alpha_o. \quad (24)$$

By a change of variables

$$\alpha_n = \alpha_0 + n\Lambda, \quad d\alpha_n = d\alpha_0, \quad (25)$$

this becomes

$$\psi_{sc}^{(n)}(x, z) = \int_{-\infty}^{\infty} B(\alpha_n - n\Lambda) R_n(\alpha_n - n\Lambda) e^{ik(\alpha_n x + \beta_n z)} d\alpha_n. \quad (26)$$

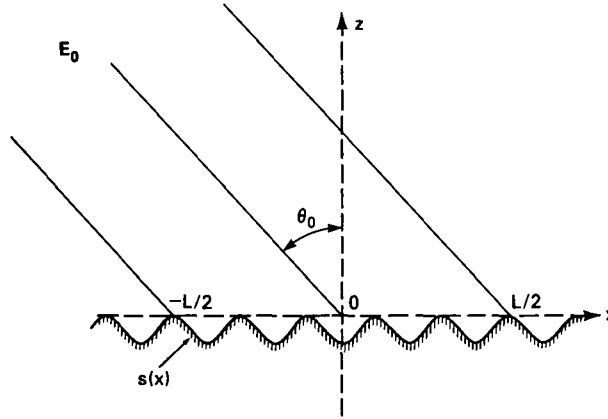


Fig. 3—Finite beam incident upon a sinusoidal surface

This integral can be evaluated for large $r = \sqrt{x^2 + z^2}$ (far field) by the method of steepest descents [21] by transforming α_n to the complex-angle plane:

$$\begin{aligned} \alpha_n &= \sin w_n, \quad \beta_n = \cos w_n, \\ x &= r \sin \theta, \quad z = r \cos \theta, \\ \alpha_n x + \beta_n z &= r \cos(w_n - \theta), \\ d\alpha_n &= \cos w_n dw_n. \end{aligned}$$

Equation (26) becomes

$$\psi_{sc}^{(n)}(x, z) = \int_p B(\sin w_n - n\Lambda) R_n(\sin w_n - n\Lambda) e^{ikr \cos(w_n - \theta)} dw_n, \quad (27)$$

where T is the contour shown in Fig. 4. Since BR_n is independent of r , the relevant saddle point for this integral is found from the condition

$$\frac{d}{dw_n} \cos(w_n - \theta) = 0, \quad (28)$$

so that

$$w_n = \theta. \quad (29)$$

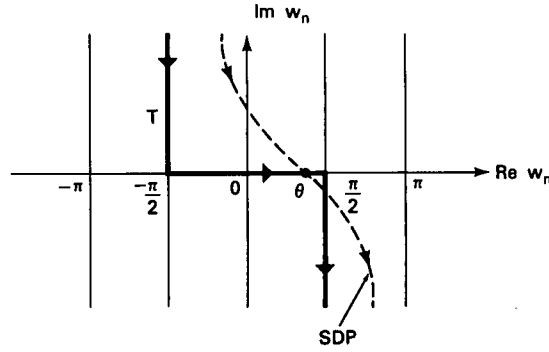


Fig. 4—Complex angle plane with contour of integration T and steepest descent path SDP

If the integral is asymptotically evaluated for large r along the steepest descent path SDP , we obtain

$$\psi_{sc}^{(n)}(x, z) = \sqrt{\frac{2\pi}{kr}} B(\sin \theta - n\Lambda) R_n(\sin \theta - n\Lambda) e^{i(kr - \pi/4)} \left[1 + O\left(\frac{1}{r}\right) \right], \quad (30)$$

for all n . The scattering pattern $S(\theta)$ can be calculated directly by using the $\psi_{sc}^{(n)}$ in the far field:

$$S(\theta) = \lim_{r \rightarrow \infty} \left(\sum_{n \in P} \psi_{sc}^{(n)} \right) \cdot \left(\sum_{n \in P} \bar{\psi}_{sc}^{(n)} \right), \quad (31)$$

where $\bar{\psi}$ means complex conjugate of ψ .

In principle it is now possible to compute $S(\theta)$ explicitly for $-\pi/2 \leq \theta \leq \pi/2$. However, an examination of Eq. (30) shows that R_n will be needed for a large number of incidence angles, making the computation of one scattering pattern quite lengthy. Equation (30) can be simplified to avoid this difficulty for illuminations which are many wavelengths wide. We consider the following nonuniform beam illumination:

$$\psi_o(x, z) = W(x/L) e^{ik(\alpha_o x - \beta_o z)} \quad (32)$$

with

$$W(x/L) = 0, \quad |x| > L/2.$$

Here $W(x/L)$ is a slowly varying function across the width of the incident beam. By using Eq. (32) in Eq. (21) and defining the Fourier transform of W as

$$Q(\sigma) = \int_{-\infty}^{\infty} W(x) e^{i\sigma x} dx, \quad (33)$$

we find

$$B(\alpha_o) = LQ[kL(\sin \theta - \alpha_o)]. \quad (34)$$

For example, if a constant illumination is assumed, i.e.,

$$W(x/L) = 1, \quad |x| < L/2, \quad (35)$$

then

$$Q(kL\sigma) = \frac{\sin \frac{kL\sigma}{2}}{kL\sigma/2}, \quad (36)$$

which becomes sharply peaked for large kL . This can be shown to be true for an arbitrary illumination when W is well behaved.

Equation (34) can now be substituted in Eq. (30) to obtain

$$\psi_{sc}^{(n)}(r) \sim \sqrt{\frac{2\pi}{kr}} LQ(kL(\sin\theta - \sin\theta_o - n\Lambda)) R_n(\sin\theta - n\Lambda) e^{i(kr - \pi/4)}, \quad (37)$$

which expresses the space-harmonic amplitude as a product of the corresponding scattering coefficient R_n and the pattern function Q . Since $\sin\theta_n = \sin\theta_o + n\Lambda$, this becomes

$$\psi_{sc}^{(n)}(r) \sim \sqrt{\frac{2\pi}{kr}} LQ(kL(\sin\theta - \sin\theta_n)) R_n(\sin\theta - n\Lambda) e^{i(kr - \pi/4)}. \quad (38)$$

When kL is large, Q becomes sharply peaked about $\theta = \theta_n$. Thus if R_n is not too rapidly varying near $\theta = \theta_n$, we can replace the $\sin\theta$ in the argument of R_n by $\sin\theta_n$. Then using the grating equation (5), we find

$$\psi_{sc}^{(n)}(r) \sim \sqrt{\frac{2\pi}{kr}} LQ(kL(\sin\theta - \sin\theta_n)) R_n(\sin\theta_o) e^{i(kr - \pi/4)}, \quad n \in P. \quad (39)$$

We note first that now the R_n are only required at the incidence angle θ_o , and second that only the set P is needed since the evanescent modes do not contribute. They do not contribute since θ_n is imaginary for $n \in E$ and the absolute value of the argument of Q , i.e. $|kL(\sin\theta - \sin\theta_n)|$, is always large for large kL . The scattering pattern is calculated by using Eq. (39) in Eq. (31):

$$S(\theta) = \left[\sum_{n \in P} Q(kL(\sin\theta - \sin\theta_n)) R_n(\sin\theta_o) \right] \times \left[\sum_{n \in P} Q(kL(\sin\theta - \sin\theta_n)) \bar{R}_n(\sin\theta_o) \right]. \quad (40)$$

Plots of $S(\theta)$ vs θ are shown in Figs. 5 to 10 corresponding to the examples of Table 1. In general a major peak is located at the scattering angle for each propagating space harmonic. The beamwidth θ_{Qn} of each major peak is found from the width of the principal maximum of the pattern function:

$$\frac{kL}{2} (\sin(\theta_o + \theta_Q) - \sin\theta_n) = \pi. \quad (41)$$

For $\Lambda \ll 1$, this becomes

$$\theta_{Qn} \approx \frac{\Lambda}{\cos\theta_n}. \quad (42)$$

If the major peaks do not interfere to a large extent, the peak values can be related to the corresponding R_n to within a normalization constant.

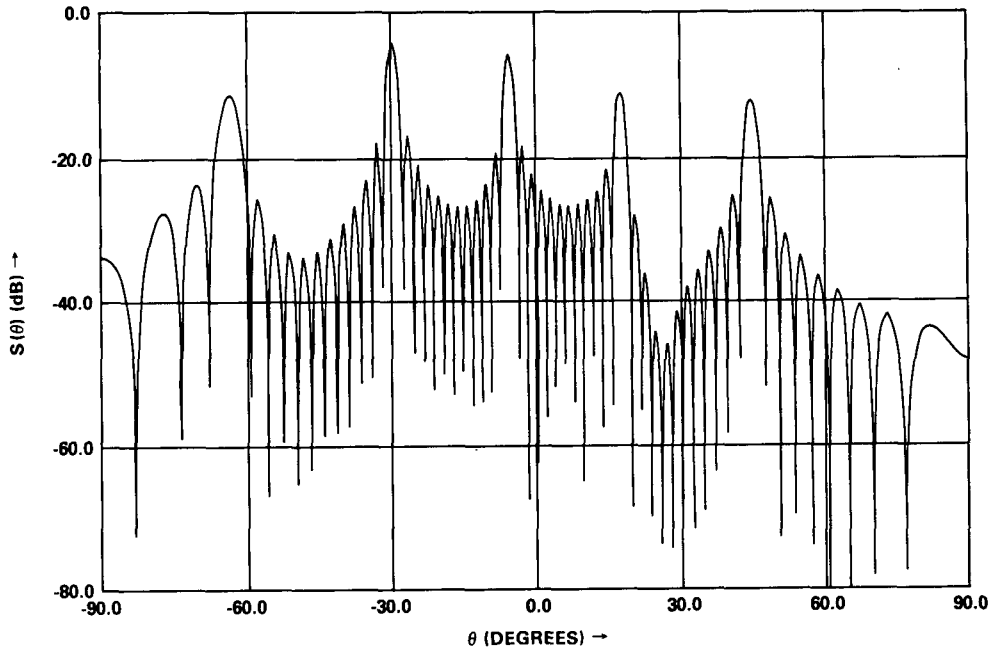


Fig. 5—Scattering pattern corresponding to Example 1:
 $\Lambda=0.40, \Delta=2.356, \theta_o=45^\circ, L/\lambda = 30$

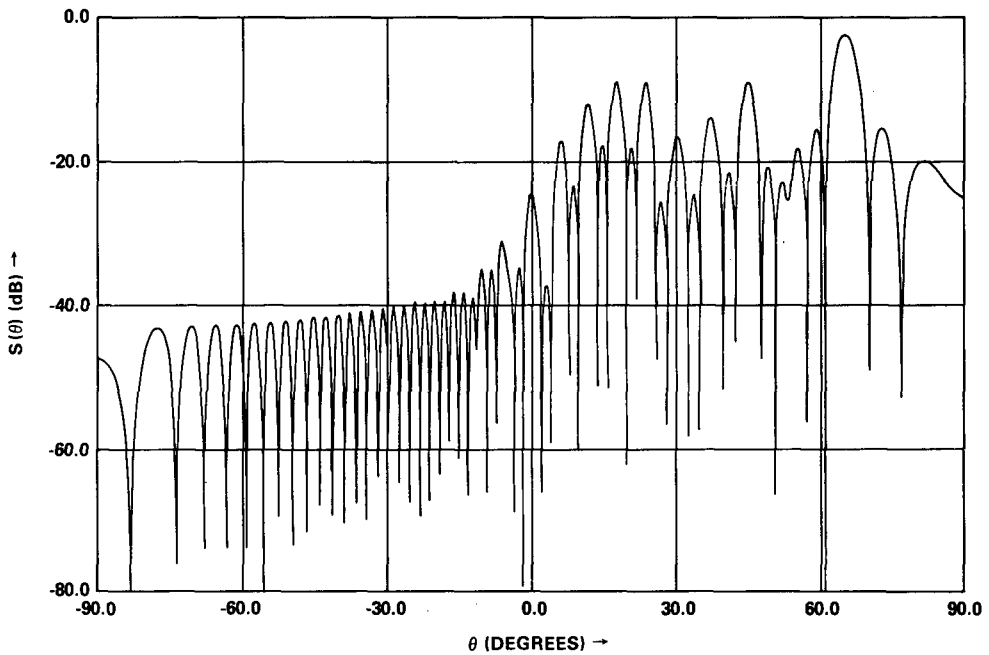


Fig. 6—Scattering pattern corresponding to Example 2:
 $\Lambda=0.10, \Delta=3.00, \theta_o=45^\circ, L/\lambda=30$

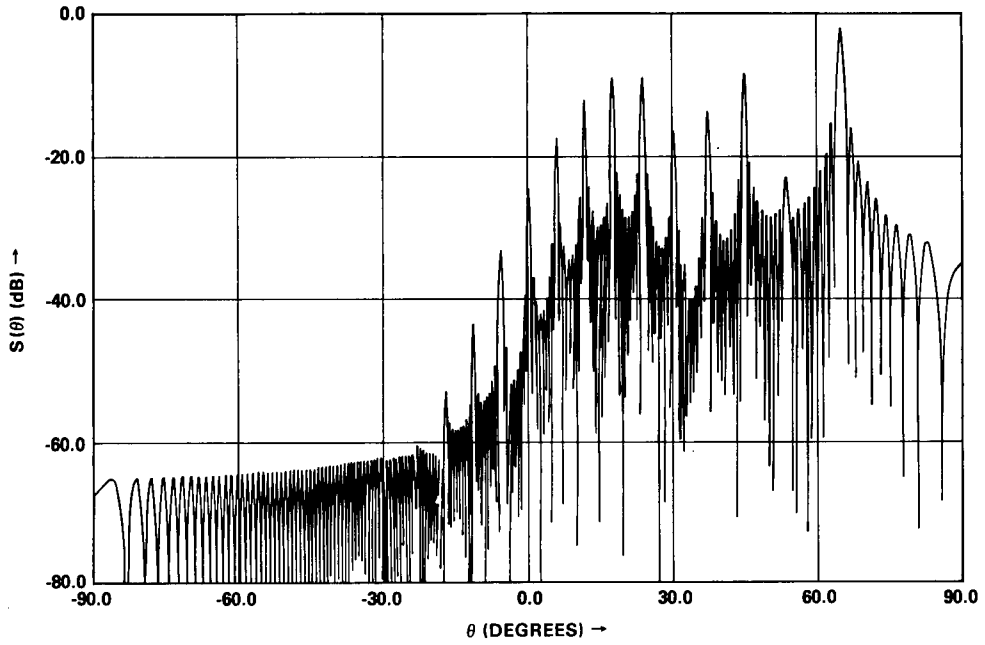


Fig. 7—Scattering pattern corresponding to Example 2: $L/\lambda = 100$

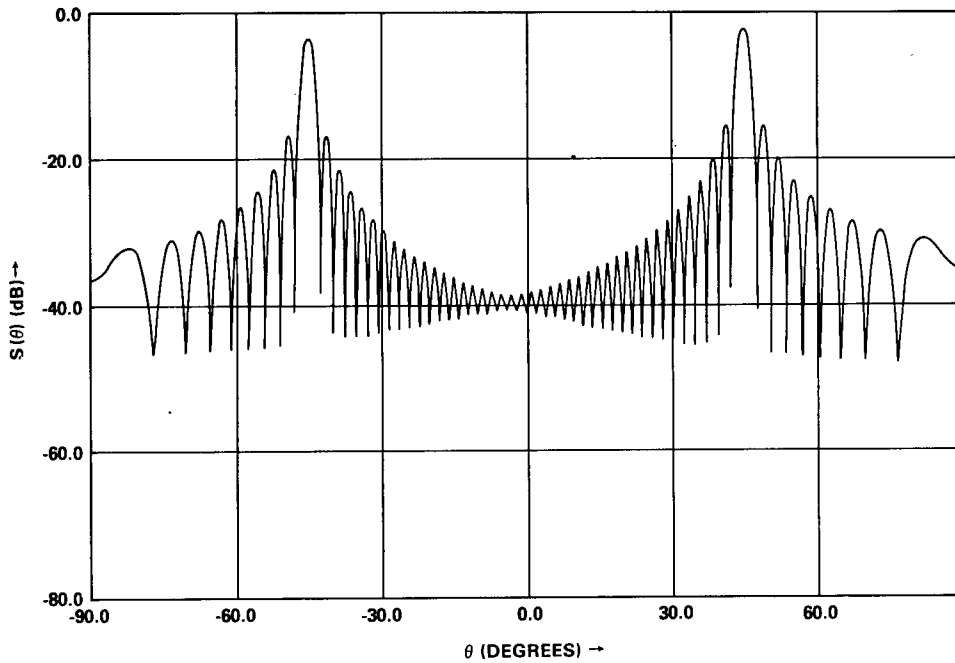


Fig. 8—Scattering pattern for first-order Bragg backscatter, Example 3:
 $\Lambda = \sqrt{2}, \Delta = 1.50, \theta_0 = 45^\circ, L/\lambda = 30$

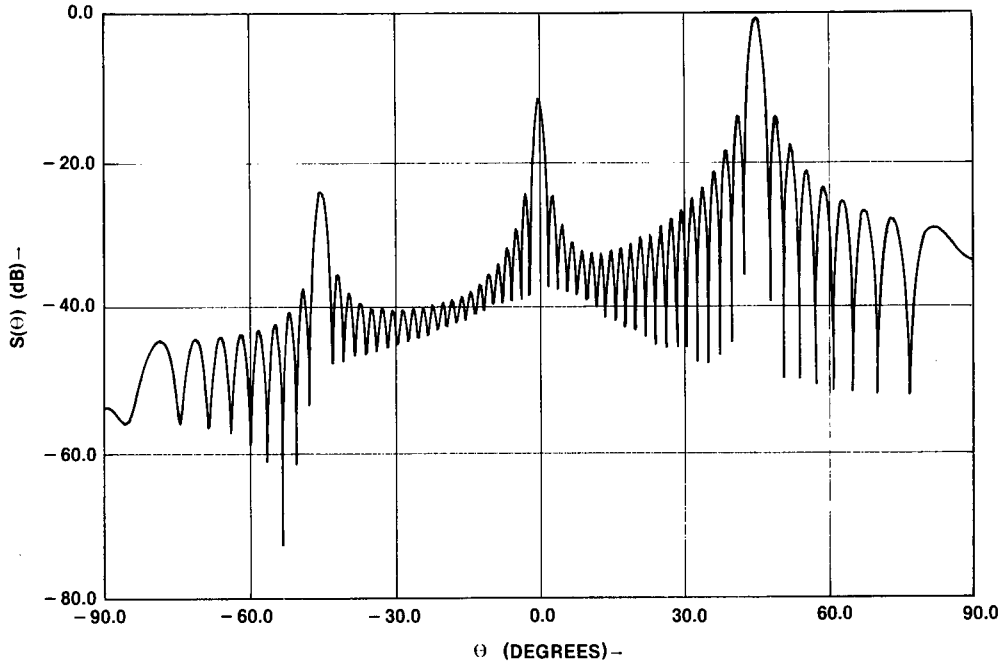


Fig. 9—Scattering pattern for second-order Bragg backscatter, Example 4:
 $\Lambda = \sqrt{2}/2$, $\Delta = 1.110$, $\theta_0 = 45^\circ$, $L/\lambda = 30$

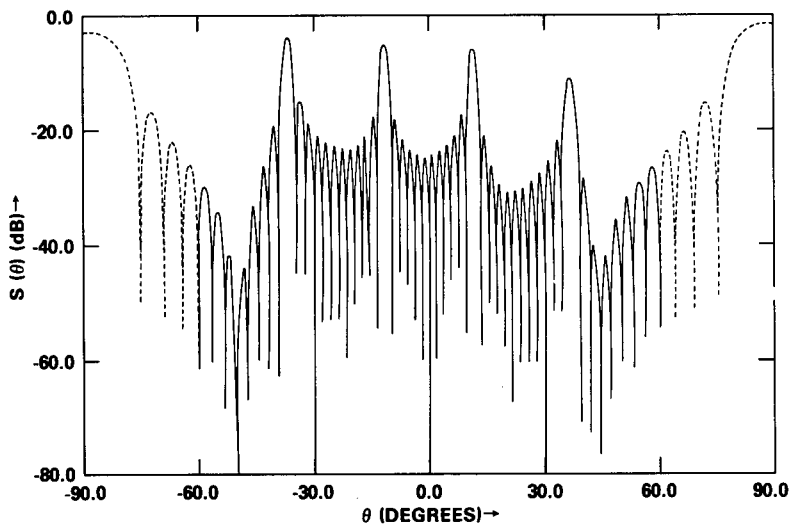


Fig. 10—Scattering pattern corresponding to Example 5: $\Lambda = 0.40$, $\Delta = 2.356$,
 $\theta_0 = 11.536^\circ$, $\lambda = 30$. The estimated pattern close to the Rayleigh-Wood angles is
 represented by dashed lines.

DISCUSSION

The scattering patterns were calculated by using the formulation (40) in terms of products of space-harmonic scattering coefficients with the corresponding pattern functions. The examples of Table 1 were considered for these calculations.

Figure 5, which corresponds to Example 1, shows five widely separated peaks whose locations agree with the corresponding space-harmonic angles and whose peak values are proportional to the corresponding reflection coefficients. The scattering lobe structure around each peak is determined by the corresponding pattern function.

Figures 6 and 7, which correspond to Example 2, show the effects of interference between several closely spaced space harmonics. Although there exist 20 propagating space harmonics, there are only 13 clearly discernible scattering peaks. The values of the peaks are different from the previously published results since we used the exact representation of the electromagnetic field. In addition, scattering patterns have been plotted for two different illuminated widths, $L/\lambda = 30$ in Fig. 6 and $L/\lambda = 100$ in Fig. 7, to demonstrate the effects of different pattern functions.

Figures 8 and 9, which correspond to Examples 3 and 4, relate the specularly reflected peak with the first- or second-order Bragg backscattered peak, since for these cases the space harmonics are widely separated.

The scattering pattern for Example 5 is partially presented in Fig. 10 since the approximation (39) is not entirely valid at the Rayleigh-Wood angles; however, it is valid at the remaining scattering angles.

The numerically economical assumption of calculating the scattering coefficients only at the incidence angle $\theta = \theta_o$ can be estimated to first order. This is done by expanding $R_n(\sin\theta - n\Lambda)$ in a Taylor series about $\theta = \theta_o$:

$$R_n(\sin\theta - n\Lambda) = R_n(\sin\theta_o) + \frac{dR_n(\sin\theta_o)}{d\theta_o} (\theta - \theta_o) + 0((\theta - \theta_o)^2), \quad (43)$$

or

$$R_n(\sin\theta - n\Lambda) \approx R_n(\sin\theta_o) [1 + \delta_1],$$

where δ_1 is the first-order estimate of the error made by replacing θ by θ_o in Eq. (38):

$$\delta_1 = \frac{(\theta - \theta_o)}{R_n(\sin\theta_o)} \frac{dR_n(\sin\theta_o)}{d\theta_o}, \quad n \in P. \quad (44)$$

To ensure that the approximation reproduces at least the major lobe associated with each space harmonic in the scattering pattern, we require that $\delta_1 \ll 1$ for $|\theta - \theta_o| < \theta_{Qn}$, or

$$\frac{1}{2 R_n(\sin\theta_o)} \frac{dR_n(\sin\theta_o)}{d\theta_o} |\theta_{Qn}| \ll 1, \quad n \in P, \quad (45)$$

where the beamwidth θ_{Qn} is calculated from Eq. (41). If R_n and its first derivative are bounded

and nonzero, then keeping θ_{Qn} sufficiently small will ensure that the error is small. However, if the incident wave is grazing along the plane $z=0$, $\left[\text{i.e. } \theta_o = \frac{\pi}{2} \right]$, or if one of the scattered space harmonics is grazing with $\theta_n = \pm \frac{\pi}{2}$ (i.e., a Rayleigh-Wood anomaly appears), then $R_n(\sin\theta_o) = 0$ and the error is unbounded. (It can also be shown that $\frac{d}{d\theta_o} R_n(\sin\theta_o)$ does not become small in both cases.) Thus the approximate expression (39) does not accurately represent the scattering pattern for grazing incidence or at a Rayleigh-Wood angle.

When the approximation (39) can no longer be used because $R_n(\sin\theta_o)$ is rapidly varying, the $R_n(\sin\theta - n\Lambda)$ must be calculated directly. To do this, we partition the angular interval $-\pi/2 < \theta < \pi/2$ into $M-1$ subintervals which in turn define the angles θ_m , $m=1, \dots, M$. The equivalent incidence angles are now defined by $\sin\theta_{omn} = \sin\theta_m - n\Lambda$, so that the space-harmonic scattering coefficients $R_n(\sin\theta_{omn})$ must now be calculated for equivalent incidence angles defined for each m and n . However, for certain m and n , $|\sin\theta_m - n\Lambda| > 1$, which correspond to imaginary angles of incidence or incident evanescent waves. Thus, a nonpropagating incident wave can excite a propagating space harmonic.

The space harmonics excited by evanescent waves are due to the complete specification of the incident beam at the surface. This complete specification includes evanescent waves which will couple directly into the surface without attenuation and, as a result, must be included in our calculations. If the source had been placed so that the surface would be in its far field, then evanescent waves excited by the source would be negligible at the surface.

Our method for scattering-pattern calculations can be compared to methods similar to those discussed in Lentz [14]. As was indicated there, point-matching techniques require several points for each electromagnetic wavelength of the illuminated area and thus are usually limited by computer storage to relatively short illuminated lengths ($< 60 \lambda$). The present method, due to the treatment of the pattern functions associated with each scattered space harmonic, does not have this limitation. However, it is limited to relatively few (< 50) scattered space harmonics and thus can be considered complementary to methods using the physical-optics approximation and point-matching techniques.

ACKNOWLEDGMENTS

The authors gratefully acknowledge several informative discussions with G. Whitman, Bell Telephone Laboratory, and J. DeSanto, N. Guinard, G. Valenzuela, and J. Wright, Naval Research Laboratory. The computer plots and Fortran programming were competently completed by Mrs. L. T. Lin.

REFERENCES

1. J.A. DeSanto, "Scattering From a Sinusoid: Derivation of Linear Equations for the Field Amplitudes," J. Acoust. Soc. Am., **57**, pp. 1195-1197, 1975.

2. J.L. Uretsky, "The Scattering of Plane Waves From Periodic Surfaces," *Ann. Phys. (New York)*, **33**, pp. 400-427, 1965.
3. K.A. Zaki and A.R. Neureuther, "Scattering From a Perfectly Conducting Surface With a Sinusoidal Height Profile: TE Polarization," *IEEE Trans. Antennas and Propag.*, **AP-19**, pp. 208-214, 1971.
4. T.C.H. Tong and T.B.A. Senior, "Scattering of Electromagnetic Waves by a Periodic Surface With Arbitrary Profile," *Univ. of Mich. Rad. Lab., Sci. Rept. No. 13, AFCRL-72-0258; N.T.I.S., AD747491*, 1972.
5. G. Whitman, and F. Schwering, "Scattering by Periodic Metal Surfaces With Sinusoidal Height Profiles — a Theoretical Approach," *IEEE Trans. Antennas and Propag.*, **AP-25**, pp. 869-876, 1977.
6. P.C. Waterman, "Scattering by Periodic Surfaces," *J. Acoust. Soc. Am.*, **57**, pp. 791-802, 1975.
7. S.O. Rice, "Reflection of Electromagnetic Waves from Slightly Rough Surfaces," *Commun. Pure Appl. Math.*, **4**, pp. 351-378, 1951.
8. G.R. Valenzuela, "Scattering of Electromagnetic Waves From a Tilted, Slightly Rough Surface," *Radio Sci.* **3**, pp. 1057-1066, 1968.
9. J.W. Wright, "Backscattering From Capillary Waves With Application to Sea Clutter," *IEEE Trans. Antennas and Propag.*, **AP-14**, pp. 749-754, 1966.
10. D.E. Barrick, "First-Order Theory and Analysis of MF/HF/VHF Scatter From the Sea," *IEEE Trans. Antennas and Propag.*, **AP-20**, pp. 2-10, 1972.
11. R.K. Rosich, and J.R. Wait, "A General Perturbation Solution for Reflection From Two-Dimensional Periodic Surfaces," *Radio Sci.*, **12**, pp. 719-729, 1977.
12. P. Beckmann and A. Spizzichino, *The Scattering of Electromagnetic Waves from Rough Surfaces*, Macmillan Co., New York, 1963.
13. T.B.A. Senior, "The Scattering of Electromagnetic Waves by a Corrugated Sheet, *Can. J. Phys.*, **37**, pp. 787-797, correction, p. 1572, 1959.
14. R.R. Lentz, "A Numerical Study of Electromagnetic Scattering From Ocean-Like Surfaces," *Radio Sci.*, **9**, pp. 1139-1146, 1974.
15. A.K. Fung and H.L. Chan, "Backscattering of Waves by Composite Rough Surfaces," *IEEE Trans. Antennas Propag.*, **AP-17**, pp. 590-597, 1969.

16. G.R. Valenzuela, "Theories for the Interaction of Electromagnetic and Ocean Waves – a Review," *Boundary-Layer Meteorology*, **13**, pp. 61-85, 1978.
17. A.B. Shmelev, "Wave Scattering by Statistically Uneven Surfaces," *Soviet Physics – Uspekhi*, **15**, pp. 173-183, 1972.
18. R.F. Millar, "The Rayleigh Hypothesis and a Related Least-Squares Solution to Scattering Problems for Periodic Surfaces and Other Scatterers," *Radio Sci.*, **8**, pp. 785-796, 1973.
19. R.L. Holford, "Scattering of Sound Waves at a Periodic Pressure-Release Surface: an Exact Solution," *Bell Tel. Labs. Tech. Rep.*, Whippany, N.J., 1971.
20. A. Hessel and A.A. Oliner, "A New Theory of Wood's Anomalies on Optical Gratings," *Appl. Optics*, **4**, pp. 1275-1297, 1965.
21. L.B. Felsen and N. Marcuvitz, *Radiation and Scattering of Waves*, Chap. 5, Prentice-Hall, Englewood Cliffs, N. J., 1973.